ORIGINAL PAPER

Nanoscale Resistive Switching in Ultrathin PbZr$_{0.2}$Ti$_{0.8}$O$_3$–La$_{0.7}$Sr$_{0.3}$MnO$_3$ Bilayer

Tino Band, Diana A. Rata, Robert Roth, Stefan G. Ebbinghaus, and Kathrin Dörr*

Electric switching of ultrathin ferroelectric films is vital for electronic elements such as multiferroic tunnel junctions, but the large required field may induce ionic motions as addressed here. Unipolar current–voltage (I–V) characteristics of ultrathin (3 nm) PbZr$_{0.2}$Ti$_{0.8}$O$_3$ (PZT) grown on La$_{0.7}$Sr$_{0.3}$MnO$_3$ (LSMO) by pulsed laser deposition have been investigated in an ambient-condition force microscope. Topographic changes have been recorded after the I–V measurements. No ferroelectric switching is found, but resistive switching with features in agreement with earlier work on similar perovskite titanates. The onset of hysteretical I–V loops is correlated with a clear height increase in the contacted area under the Pt-covered tip. The onset voltage of 4.5 V (−2.5 V) for positive (negative) tip bias is clearly different for the two voltage polarities. The observed height changes after applying electrical voltage reveal a volume expansion that must be attributed to chemical changes in both the PZT and the LSMO layers. A fast and a slow process of ionic motion or electrochemical reaction contributing to the observed features is identified. The slow one occurs at negative voltage, causes very large height increase, and is hypothetically attributed to processes following the electro-splitting of the adsorbed surface water.

1. Introduction

Electron tunneling through a ferroelectric barrier has received increasing interest in recent years because the polarization in the barrier was found to control the tunneling current.[1–11] Early work on tunneling through a ferroelectric started with theoretical considerations.[1] Multiferroic four-state tunnel junctions have been introduced by combining the ferroelectric barrier with

T. Band, Dr. D. A. Rata, R. Roth, Dr. K. Dörr
Institute of Physics
Martin Luther University Halle-Wittenberg
Halle 06099, Germany
E-mail: kathrin.doerr@physik.uni-halle.de

Dr. S. G. Ebbinghaus
Institute of Chemistry
Martin Luther University Halle-Wittenberg
Halle 06099, Germany

spin-polarized tunneling in magnetic tunnel junctions.[5,7,11] Both BaTiO$_3$ and PbZr$_x$Ti$_{1−x}$O$_3$ (PZT, $x = 0$–0.5) have been used as ferroelectric for the tunnel barrier.[8–11]

For proper function as a tunnel barrier, ferroelectric layers of about 1–5 nm thickness need to be reversibly switched. This poses the challenge of applying very large electric fields to the barrier, because the coercive fields of ferroelectric films grow strongly with reduced thickness.[12] Often, the required electric field is of the order of 1–10 MV cm$^{−1}$. An electric field of this magnitude can drive processes which are of electrochemical nature and change the chemical composition in or near the tunnel barrier. Such phenomena are part of another very active research area: resistive switching based on voltage-driven ionic movements has been vastly explored for memory applications in the last 15 years.[13] Until now, ferroelectric PbZr$_x$Ti$_{1−x}$O$_3$ (PZT, $x = 0$–0.5) has very rarely been studied with respect to resistive switching based on ionic motions. Choi et al. measured electrical transport and switching of PZT ($x = 0.3$) capacitors with a Pt (top) and a La$_{0.5}$Sr$_{0.5}$CoO$_3$ (bottom) electrode, varying the thickness of the PZT layer between 17 and 160 nm.[14] They found bipolar resistive switching instead of a polarization reversal for a PZT thickness of ≤ 34 nm. The characteristics of bipolar resistive switching can be described as follows: during cycling the voltage applied to the Pt electrode from zero to positive maximum, negative maximum, and back to zero, the resistance drops at a positive threshold voltage indicating a transition to a so-called low-resistance state (LRS). The LRS turns back to the high-resistance state (HRS) at a negative threshold voltage. The current versus voltage (I–V) loop thus roughly follows the shape of the number eight, starting with a counterclockwise loop at positive voltages. (Our measurements presented here are unipolar; nevertheless, **Figure 1**b can be used for an impression of how the positive half of the bipolar I–V loop would look like.) The work of Choi et al. showed that thin PZT layers display similar bipolar resistive switching such as SrTiO$_3$ which has often been studied and utilized in resistive switching elements.[15–17] Qin et al. studied tunnel barriers made of PZT and BaTiO$_3$ as well as dielectric SrTiO$_3$ in nominally symmetric electrode configurations with LSMO on both sides and find bipolar resistive switching without polarization reversal.[18] All three titanates show similar behavior despite their different electric nature. Notably, the application of a positive threshold voltage
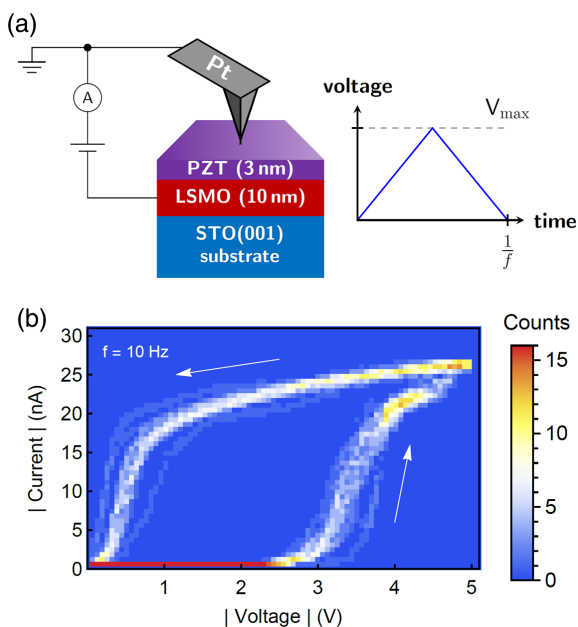
Figure 1. a) Schematic sample with force microscopy tip and unipolar voltage cycle; b) example of 16 current–voltage loops measured with same maximum voltage at 16 different positions.

drives a transition to HRS in that work. The authors propose electric-field-driven oxygen vacancy migration in the barrier including an interface-near electrode layer as probable origin of the observed resistive switching. The same group of researchers imaged structural phase transitions occurring during removal of oxygen from a LSMO layer in a transmission electron microscope; they studied in situ resistive switching in the electric field of a biased tip.[19]

Piezoresponse force microscopy (PFM) and conducting atomic force microscopy (C-AFM) have played a prominent role in recent investigations of ferroelectric tunnel barriers.[6–9] A small area of a ferroelectric layer is electrically poled using PFM and the resulting conductivity change is mapped using C-AFM. This enables direct correlation of electrical conduction with polarization orientation on the nanoscale. Local I–V characteristics can be measured at fixed position of the conducting tip with a lateral resolution of about 20–60 nm depending on the tip radius. The I–V curves have been used to evaluate the tunnel barrier parameters to identify changes after switching the ferroelectric polarization.[6,9,20] In addition, I–V curves can be hysteretic due to 1) ferroelectric switching or 2) as a consequence of ion transport in the electric field.[21] In a force microscope, the surface topography can be simultaneously imaged. Some of the experiments revealed an irreversible height increase under the tip ranging from 0.3 nm to several 10 nm after application of a large electric field. The detection of surface modification clearly reveals a transport of material. Kalinin et al. gave an overview on ionic transport mechanisms which may be involved in PFM.[22] In particular, electrical modes of force microscopy used under ambient conditions may suffer from effects caused by an adsorbate layer of water on the sample surface that is involved in the tip-induced electrochemical processes.

This work aims at improving the knowledge on processes which occur during electric switching of ultrathin PZT in a force microscope. We find characteristics typical of resistive switching and study them using electrical and topographic measurements. (We note that this work is not intended as a suggestion of another resistive switching element, but motivated by the elucidation of processes occurring during switching of ultrathin ferroelectric films required in electronic elements such as tunnel junctions.) Unipolar I–V characteristics with both positive and negative voltages have been recorded separately to investigate the influence of voltage polarity. Different voltage cycling frequencies between 0.1 and 10 Hz have been applied to discriminate between slower and faster processes. Resistive switching without polarization reversal has been observed in a 3 nm-thick PZT ($x = 0.2$) film. Several features are found to be similar to those of resistive switching in $SrTiO_3$. For negative tip voltages, we find a relatively fast process underlying I–V loops with counterclockwise hysteresis and a slower process which is associated with clockwise I–V hysteresis. The latter dominates at larger magnitude of voltages. Associated with the hysteresis at larger voltages is a huge height expansion (≤ 40 nm) under the tip. In contrast, positive tip polarity in the same range of voltages results in moderate surface deformation (≤ 2.5 nm) with stable logarithmic height increase over time and weak frequency dependence. The faster ionic process present for both tip polarities is tentatively attributed to oxygen vacancy transport which can explain a height increase of < 5 nm if one assumes that the LSMO bottom electrode participates in the oxygen transport. The slower process is responsible for vast dot heights of up to 40 nm observed at large negative tip voltages and small frequency (0.1 Hz). This process is hypothetically attributed to decomposing the surface water layer with subsequent chemical reactions in the oxide layers.

2. Experimental Section

A bilayer sample consisting of 3 nm PZT and 10 nm LSMO (bottom electrode) was grown epitaxially on a (001)-oriented $SrTiO_3$ substrate by pulsed laser deposition (PLD) using a KrF laser (wavelength 248 nm). Each film was deposited in 0.1 mbar of oxygen with a laser frequency of 2 Hz. Substrate temperature and laser energy density were 575 °C and 0.6 J cm^{-2} for PZT and 700 °C and 1 J cm^{-2} for LSMO, respectively. After deposition, the sample was annealed for 30 min at 575 °C in 200 mbar O_2, followed by cooling to room temperature with a cooling rate of 10 K min^{-1}. Film thickness and lattice structure were evaluated by high-resolution X-ray diffraction (XRD) in a Bruker D8 Discover diffractometer.

A commercial atomic force microscope (AFM, NT-MDT NTEGRA Aura) was used to measure the surface topography and local I–V characteristics under ambient conditions with Pt-coated Si tips (HQ:NSC18/Pt, MikroMasch). The tip radius was about 30 nm. I–V measurements in fixed tip positions were conducted by applying a unipolar linear voltage sweep between the Pt-covered tip and the LSMO bottom electrode as shown in Figure 1a. The maximum voltage (V_{max}) was varied from 2 to 6 V for positive tip bias and from -2 to -5 V for negative tip bias. Sweep frequencies of 0.1, 1, and 10 Hz were applied. Single-point measurements at fixed sweep frequency were done on a

16×16 grid in a $5 \times 5\,\mu m^2$ area, where a row consisting of 16 points was measured for each V_{max}. After this electrical measurement, the surface change was imaged with AFM semicontact (tapping) mode. The loop area of the hysteretic current–voltage curve, calculated as integral of $I(V)dV$ over the complete voltage cycle, and the surface height increase in the contact area were represented as the median value obtained from the 16 I–V runs. Note that a positive (negative) loop area per aforementioned definition means a clockwise (counterclockwise) sense of the I–V loop. Error bars show the lower and upper quartile.

3. Results and Discussion

The PZT (3 nm)/LSMO (10 nm) bilayer has been grown coherently on STO(001) with an in-plane lattice parameter of 3.905 Å. The root-mean-square (rms) surface roughness determined in the measured area is 0.24 nm. Ferroelectric switching has been tested by writing circular domains with both tip voltage polarities and subsequent measurement of the vertical piezoresponse. No ferroelectric switching could be observed at any tip voltages between -5 and 6 V. These voltages induce large nominal electric fields between -16 and 20 MV cm^{-1}, respectively, in the PZT layer. After writing, the PZT film showed dots protruding from the film surface (**Figure 2**a,b). The height of these "written" dots increased with the magnitude of the voltage indicating local chemical changes of the PZT film caused by the applied electric field. Therefore, FE switching could not be achieved because the required field drives chemical processes.

To gain more insight into the nature of the field-induced processes, I–V loops have been systematically recorded at three

frequencies as described in Section 2 and the height of the resulting dots has been measured. Figure 2 shows the topography of a representative set of dots in a 16×16 dot array (Figure 2a) and an enlarged section (Figure 2b). Figure 2c contains a representative line scan across dots which is marked in Figure 2b. Strikingly, some dots written at large tip voltage reach considerable heights of up to $\approx$40 nm. The material for the huge dots must come from the surrounding film because the Pt-covered tip was not affected. There are two potential scenarios: 1) the material in the dots may have about the same density as the film (meaning the density of the stoichiometric perovskite phase, either in PZT or LSMO) and 2) there may be a density reduction in the dot volume. For the case of constant density (1), one can estimate the required film volume around the dot which needs to be moved into the dot. (Note that one can exclude a participation of the highly insulating substrate in any electrochemical process because there is no voltage drop expected.) Figure 2d shows the geometry with a concentric circular trench around the dot. We assume a trench width (r_2–r_1) equal to the tip radius of $\approx$30 nm because such a trench would clearly be undetectable with the same tip (Figure 2d). Using the volumes of the dot ($h_{dot}\ \pi r_1^2$) and the 13 nm-thick PZT + LSMO bilayer in the trench area (13 nm· $\pi(r_2^2-r_1^2)$), one estimates $h_{dot} \leq 40$ nm. Therefore, the density conservation scenario is consistent with the apparent absence of a depression or trench due to the lateral resolution limit from the tip radius. According to scenario 2, the anticipated chemical changes are likely to reduce the density inside the dot. Another crystalline phase with lower density may be formed or amorphous phase may be present and, ultimately, the presence of a void cannot be excluded without a cross-section image.
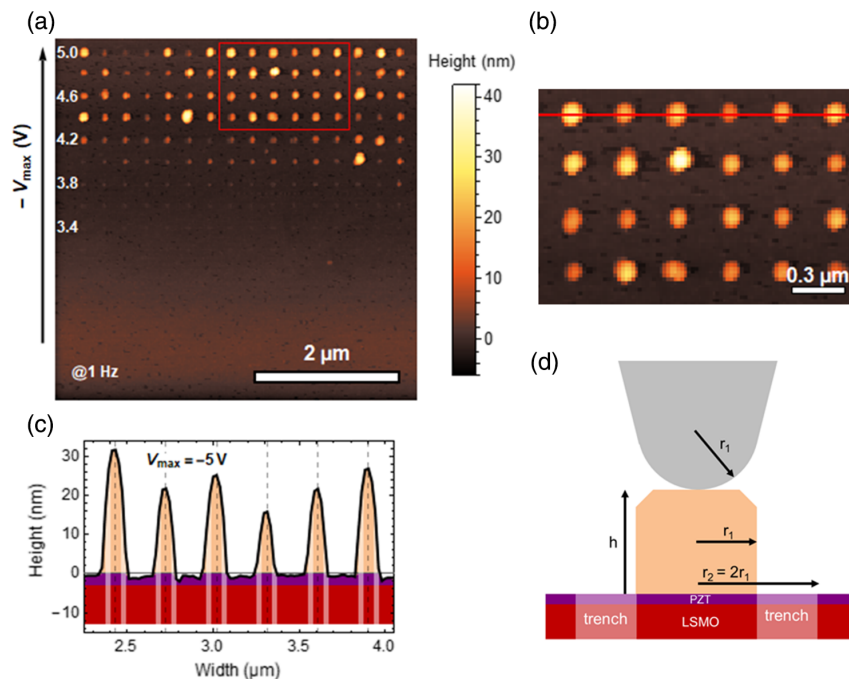

Figure 2. a) Topography image taken by atomic force microscopy after writing a 16×16 grid of dots with V_{max} increasing from bottom line to top line of dots. b) Enlarged part of (a) as marked by the yellow rectangle. c) Example for a line scan across dots. d) Schematic cross-section of a dot and surrounding film area. The trench radius of $2r_1$ means invisible trenches with a tip of radius r_1.
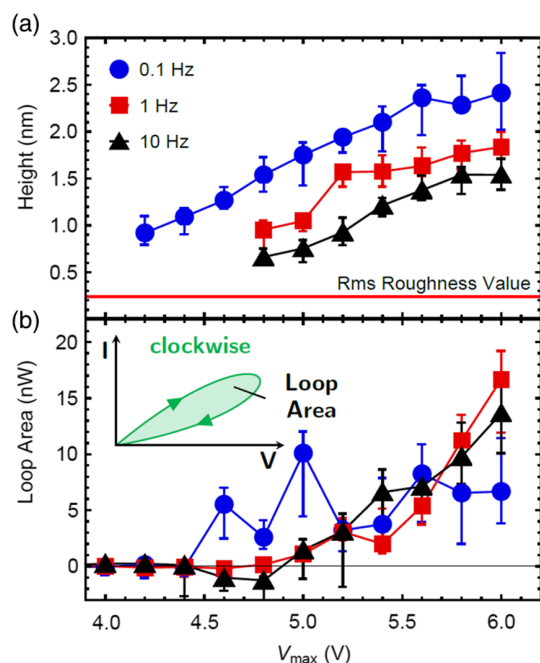
Figure 3. a) Height of written dots after the I–V measurement versus maximum voltage. As-grown rms roughness indicated. b) Loop area of the I–V curve versus maximum voltage. For the clockwise sense of the I–V loop, the loop area is positive.

Figure 4. a) Height of written dots after the I–V measurement versus V_{max} for negative voltages. As-grown rms roughness and maximum dot height for positive voltages indicated. b) Loop area of the I–V curve versus V_{max}. For the clockwise (counterclockwise) sense of the I–V loop, the loop area is positive (negative). c) Evolution of I–V loop types with measuring frequency.

Results of I–V and dot height measurements for positive tip bias are shown in **Figure 3**. The inset of Figure 3b shows a schematic I–V loop of clockwise rotation sense which is characteristic for positive tip bias in the measured voltage range. The current is smaller at the branch of decreasing voltage, resulting in a positive loop area (as defined in Section 2). The loop area is shown as a function of the maximum voltage in Figure 3b. Up to $V_{max} = 4.5$ V, the observed I–V loop area is zero, indicating reversible I–V loops and, thus, a stable state. From 4.5 to 6 V, the loop area grows with V_{max} and reaches a maximum of ≈ 17 nW. Therefore, electrochemical changes are present above 4.5 V. (If they occurred below 4.5 V, they would be reversible and, thus, harder to detect.) The loop area grows roughly exponentially with V_{max}, as would be expected for a voltage-activated mechanism. The curves of the loop area versus V_{max} essentially fall on top of each other for frequencies of 0.1, 1, and 10 Hz, apart from some additional scattering in the 0.1 Hz data which may be caused by contact instabilities during the measurement at the lowest frequency. This indicates that the processes taking place during the I–V measurement at positive voltages are fast enough to follow the voltage sweep.

The height of the written dots (Figure 3a) reveals a continuous growth of dots when the tip voltage is applied for longer time, that is, at a lower frequency. However, the height is less than doubled at 0.1 Hz compared with its value at 10 Hz, showing that the major topographic change occurs immediately (on the applied time scale). Later, we show that dots grow approximately logarithmically with time (cf. Figure 5a below). The dot height increases monotonically with V_{max} and reaches 2.4 nm at $V_{max} = 6$ V.
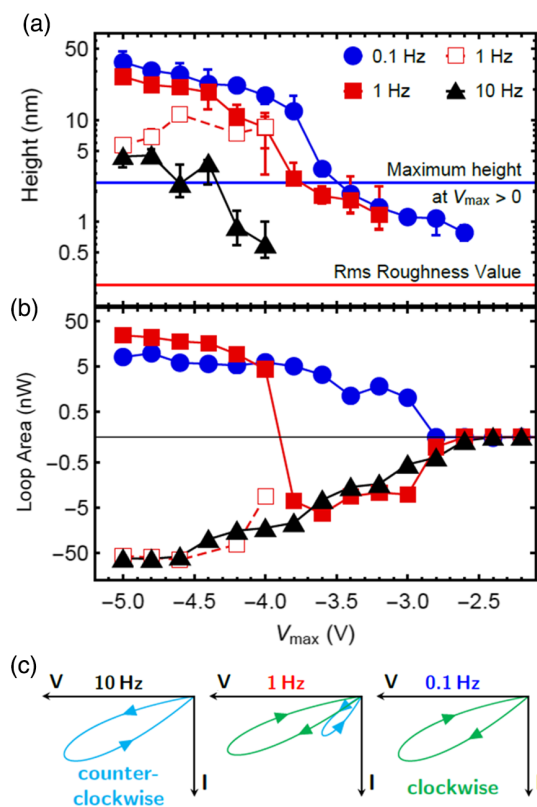
The same experiment for negative tip bias is shown in **Figure 4** and reveals a more complex behavior. The I–V loops start to be hysteretic near $|V_{max}| = 2.5$ V, a considerably lower voltage magnitude than in the case of positive tip bias. Therefore, the onset of electrochemical processes is clearly at lower voltages for a negatively biased tip. Importantly, the character of the I–V loops systematically changes with both V_{max} and the measuring frequency as shown in the schemes of Figure 4c. At the largest frequency (10 Hz), the loop runs counterclockwise as the example shown in Figure 1b, meaning the loop area is negative (Figure 4b). At 1 Hz, there is a crossover from negative to positive loop area near -3.8 V (Figure 4b). About a quarter of the loops still show a negative loop area at larger voltage magnitudes (open symbols). For this reason, two curves have been included for 1 Hz in Figure 4a,b. Most of the 1 Hz I–V loops run clockwise at larger voltages V_{max} and counterclockwise at smaller V_{max} (Figure 4c). At 0.1 Hz, positive loop area and clockwise loop sense are found at $|V_{max}| \geq 3$ V. Summarizing, the clockwise loop appears above a certain threshold voltage for a fixed frequency. This indicates a process that becomes dominating at high voltages. The process is slower than the one causing the counterclockwise loops because it can be suppressed by increasing the measuring frequency at constant V_{max}.

ADVANCED
SCIENCE NEWS
www.advancedsciencenews.com

physica
status
solidi
b
www.pss-b.com

An exponential increase in the negative loop area with V_{max} is found which covers three orders of magnitude from -0.1 to -100 nW, with a tendency of saturation above 4.6 V (Figure 4b). The obtained maximum value of the negative loop area is about -100 nW which is nearly an order of magnitude larger than for positive tip bias. The curve representing the positive loop area (recorded at 0.1 Hz, with high-voltage data points from 1 Hz runs) exhibits an onset at 3 V, followed by a continuous increase with V_{max} toward a value of ≈ 15 nW which is similar to the maximum loop area obtained at positive tip bias.

The height of written dots versus V_{max} (Figure 4a) confirms the strong impact of the negative tip polarity. Extremely large dot heights up to 40 nm have been observed at $V_{max} = -5$ V, indicating massive local transport of material. There is an onset of the very large dot heights between -3.5 and -4 V. The dots written at 10 Hz, however, remain below 4 nm up to 5 V, indicating a slow process for the immense height growth. **Figure 5** shows the dot height as a function of a growth time defined as $\tau = 1/f$ for positive and negative voltages. Over two decades of frequency, a linear relation of the height with the logarithmic growth time is found. This indicates a typical growth process of $h = A + B \log \tau$, with the dot height h and constants A and B. The slope B which determines the growth rate remains nearly constant for the different positive voltages, whereas it is larger and strongly increases with V_{max} for negative voltages. (The negative voltages ($|V_{max}| \geq 4$ V) shown in Figure 5b induce large heights of ≥ 10 nm of the written dots for $\tau = 1$ or 10 s.)

These experimental findings lead to the generalized results summarized here and discussed in detail in the following paragraphs. 1) The hysteresis of I–V loops (i.e., the nonzero loop area) and the detectable irreversible height increase after the I–V measurement set in at about the same critical voltage V_c. This indicates that both features are linked and reflect the same irreversible ionic motion processes. The value of V_c is clearly different for the tip polarities, ≈ -2.5 V for negative and ≈ 4.5 V for positive tip bias have been derived from 1 Hz and 10 Hz data in Figure 3 and 4 (which are less scattered than 0.1 Hz data). Neglecting voltage drops at the interfaces, the electric fields in the ferroelectric layer caused by the critical voltage would be -8.3 and 15 MV cm^{-1}, respectively. 2) The evolution of the type of I–V loops with growing frequency and voltage is in close resemblance to data from resistive switching elements of $SrTiO_3$ reported by several groups.[15–17,23] 3) The observed topography changes after applying electrical voltage reveal a large volume expansion that cannot be attributed to chemical changes in the thin ferroelectric layer alone. Thus, the LSMO bottom electrode must be involved in the electrochemical processes. 4) There are at least two different ionic processes involved. The faster one is observed at both tip polarities and has characteristics consistent with oxygen vacancy motion. The slower one is responsible for the vast dot heights observed at large negative tip voltages.

Kubicek et al. reported on resistive switching elements of 5 nm $SrTiO_3$ sandwiched between Pt (80 nm) and $LaNiO_3$ (10 nm) electrodes grown coherently on $LaAlO_3$(001) substrates (apart from the Pt top electrode).[15] They observe I–V characteristics in a slightly smaller range of the nominal electric field in the titanate layer (3–8 MV cm^{-1}, better defined in their case because of two stable metal electrodes instead of a force microscopy tip) and find the same crossover from counterclockwise to clockwise I–V loops with increasing maximum voltage or reduced speed of the voltage scan such as in our experiment at negative tip voltages. Voltages are applied to the Pt electrode in all discussed examples. The same reversal of the sense of I–V loops with increasing maximum voltage at a Pt electrode has also been described in a Pt/$SrTiO_3$(Fe) (500 nm)/Nb:$SrTiO_3$(001) device by Münstermann et al.,[17] but in this work, the voltage cycle started with *negative* voltages. Lee et al. showed that both bipolar I–V loop types, ("eight-wise" and "anti-eight-wise") can result from shifting the distribution of oxygen vacancies in $SrTiO_3$.[16] Whether a contact undergoes switching to a higher or a lower resistance state in the first part of a bipolar voltage cycle, that is, a clockwise or anticlockwise I–V loop, depends on its original vacancy distribution. Based on this, one may expect equally prepared resistive switching elements to show opposite loop senses in unipolar cycles of positive and negative voltages. This feature is well reproduced in our data at frequencies of 10 Hz and, in part, 1 Hz (Figure 3 and 4), whereas at 0.1 Hz, a different electrochemical process dominates the negative-voltage data as discussed later.

The observed volume changes are indicative of a participation of the bottom electrode in the chemical changes because the thickness of PZT (3 nm) is one order of magnitude smaller than the height of the written dots. Large oxygen vacancy concentrations in the lattice of PZT may cause a volume increase in the order of 25%, ruling out an oxygen vacancy redistribution in the PZT layer as the only source of the observed volume increase. The Pt tip seems to be rather unaffected in the course of experiments because many dots have been measured without decaying performance in I–V measurements.[19] Therefore, an involvement of the LSMO bottom electrode is likely.
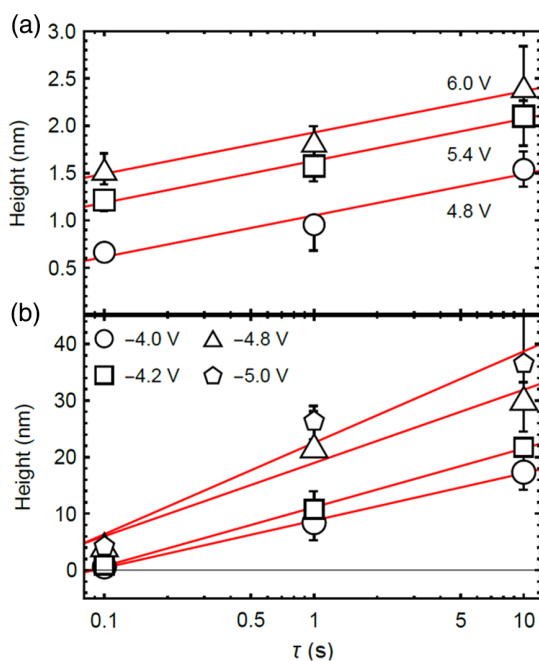

Figure 5. Dot height versus writing time $\tau = 1/f$ (frequency f) for the indicated values of V_{max} with a) positive and b) negative V_{max}.

ADVANCED
SCIENCE NEWS
www.advancedsciencenews.com
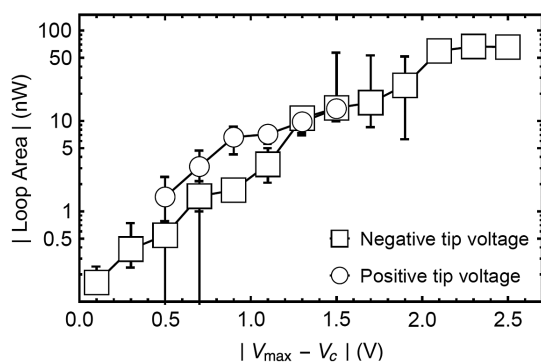
physica
status
solidi b

www.pss-b.com

Figure 6. Magnitude of the loop area versus reduced V_{max} for both voltage polarities. For negative voltages, only the branch of negative loop area associated with the fast process discussed in the text is shown. V_c denotes the smallest voltage magnitude where the loop area is not zero.

Our data suggest contributions from (at least) two different chemical processes. Volume expansion due to oxygen removal from PZT as well as from the bottom electrode[18] could account for the dots with heights of ≤ 2.5 nm. Motion of oxygen vacancies is the likely origin of the fast process observed for all positive voltages and dominating at 10 Hz (and, in part, at 1 Hz) for negative voltages. This idea is supported by the observation that, after subtracting V_c from the applied maximum voltage, loop area data for both voltage polarities reasonably coincide in this regime (**Figure 6**). In contrast, the extremely high dots obtained at large negative tip voltages occur when the $I–V$ loop area is positive. This correlation is seen best in Figure 4a,b for the branching curves recorded at 1 Hz. We suggest a hypothetical process related to electrolytic splitting of the water surface layer which may be seen as a basis for further exploration: $H_2O + e^- \rightarrow \frac{1}{2}H_2 + OH^-$.[24] Hydroxyl ions could be driven into the film surface by the large negative tip field and react with PZT to form $Pb(OH)_2$. If there is also carbon on the surface (e.g., in adsorbed CO_2), the more stable $PbCO_3$ may be formed. In the extreme case, metallic Pb could be formed, but the expected electrical conductivity enhancement arising from a metallic Pb filament has not been observed. The decisive role of the water surface layer could be checked in a repetition of the $I–V$ measurements in a vacuum force microscope. In the present stage, we have no hypothesis about possible chemical reactions in the LSMO electrode layer.

4. Conclusions

Ultrathin (3 nm) ferroelectric PZT films grown on LSMO/ $SrTiO_3(001)$ show resistive switching such as other titanates ($SrTiO_3$ and $BaTiO_3$). We have confirmed this in nanoscale force microscopy measurements of current–voltage loops at fixed tip positions with subsequent detection of topographic changes. Using a force microscopy tip enables the correlation of topographic changes resulting from ionic motion with the features of current–voltage characteristics. We find an onset of hysteretical $I–V$ behavior correlated with a clear height increase in the contacted area under the tip at a critical voltage of ≈ 4.5 V (-2.5 V) for positive (negative) tip bias. The evolution of the type of $I–V$ loops with growing frequency and voltage is in close resemblance to data from resistive switching elements of $SrTiO_3$ reported by several groups.[15,17] The observed topography changes after applying electrical voltage reveal a large volume expansion that cannot be attributed to chemical changes in the thin ferroelectric layer alone, but the LSMO bottom electrode must be involved in the electrochemical processes. There are at least two different ionic processes contributing to the observed features. The faster is active at both tip polarities and has characteristics consistent with oxygen vacancy motion. The slower induces vast dot heights up to 40 nm at large negative tip voltages and the smaller frequencies of 0.1 and 1 Hz. This process is hypothetically attributed to decomposing the surface water layer and inserting hydroxyl ions into the PZT film, and probably the LSMO electrode, where they drive chemical reactions. The water splitting could be suppressed in an ultrahigh vacuum force microscope or in resistive switching elements with a Pt top electrode layer, even though moisture still has substantial impact on such layered elements with fixed electrodes.[25]

Conflict of Interest

The authors declare no conflict of interest.

[1] L. Esaki, R. B. Laibowitz, P. J. Stiles, *IBM Tech. Discl. Bull.* **1971**, *13*, 114.
[2] J. R. Contreras, H. Kohlstedt, U. Poppe, R. Waser, *Appl. Phys. Lett.* **2003**, *83*, 4595.
[3] H. Kohlstedt, N. A. Pertsev, J. Rodríguez Contreras, R. Waser, *Phys. Rev. B* **2005**, *72*, 125341.
[4] E. Y. Tsymbal, H. Kohlstedt, *Science* **2006**, *313*, 181.
[5] M. Gajek, M. Bibes, S. Fusil, K. Bouzehouane, J. Fontcuberta, A. Barthélémy, A. Fert, *Nat. Mater.* **2007**, *6*, 296.
[6] A. Gruverman, D. Wu, H. Lu, Y. Wang, H. W. Jang, C. M. Folkman, M. Ye. Zhuravlev, D. Felker, M. Rzchowski, C-B. Eom, E. Y. Tsymbal, *Nano Lett.* **2009**, *9*, 3539.
[7] V. Garcia, S. Fusil, K. Bouzehouane, S. Enouz-Vedrenne, N. D. Mathur, A. Barthélémy, M. Bibes, *Nature* **2009**, *460*, 81.
[8] P. Maksymovych, S. Jesse, P. Yu, R. Ramesh, A. P. Baddorf, S. V. Kalinin, *Science* **2009**, *324*, 1421.
[9] P. Maksymovich, M. Pan, P. Yu, R. Ramesh, A. P. Baddorf, S. V. Kalinin, *Nanotechnology* **2011**, *22*, 254031.
[10] A. Crassous, V. Garcia, K. Bouzehouane, S. Fusil, A. H. G. Vlooswijk, G. Rispens, B. Noheda, M. Bibes, A. Barthelemy, *Appl. Phys. Lett.* **2010**, *96*, 042901.

[11] D. Pantel, S. Goetze, D. Hesse, M. Alexe, *Nat. Mater.* **2012**, *11*, 289.

[12] H. F. Kay, J. W. Dunn, *Philos. Mag.* **1962**, *7*, 2027.

[13] R. Waser, M. Aono, *Nat. Mater.* **2007**, *6*, 833.

[14] J. Choi, J.-S. Kim, I. Hwang, S. Hong, I.-S. Byun, S.-W. Lee, S.-O. Kang, B. H. Park, *Appl. Phys. Lett.* **2010**, *96*, 262113.

[15] M. Kubicek, R. Schmitt, F. Messerschmitt, J. L. M. Rupp, *ACS Nano* **2015**, *9*, 10737.

[16] S. Lee, J. S. Lee, J.-B. Park, Y. K. Kyoung, M.-J. Lee, T. W. Noh, *APL Mater.* **2014**, *2*, 066103.

[17] R. Muenstermann, T. Menke, R. Dittmann, R. Waser, *Adv. Mater.* **2010**, *22*, 4819.

[18] Q. H. Qin, L. Äkäslompolo, N. Tuomisto, L. Yao, S. Majumdar, J. Vijayakumar, A. Casiraghi, S. Inkinen, B. Chen, A. Zugarramurdi, M. Puska, S. V. Dijken, *Adv. Mater.* **2016**, *28*, 6852.

[19] L. Yao, S. Inkinen, S. V. Dijken, *Nat. Commun.* **2017**, *8*, 14544.

[20] A. Rana, H. Lu, K. Bogle, Q. Zhang, R. Vasudevan, V. Thakare, A. Gruverman, S. Ogale, N. Valanoor, *Adv. Funct. Mater.* **2014**, *24*, 3962.

[21] E. Strelcov, Y. Kim, S. Jesse, Y. Cao, I. N. Ivanov, I. I. Kravchenko, C-H. Wang, Y-C. Teng, L-Q. Chen Y. H. Chu, S. V. Kalinin, *Nano Lett.* **2013**, *13*, 3455.

[22] S. V. Kalinin, S. Jesse, A. Tselev, A. P. Baddorf, N. Balke, *ACS Nano* **2011**, *5*, 5683.

[23] Y. S. Kim, J. Kim, M. J. Yoon, C. H. Sohn, S. B. Lee, D. Lee, B. C. Jeon, H. K. Yoo, T. W. Noh, A. Bostwick, E. Rotenberg, J. Yu, S. D. Bu, B. S. Mun, *Appl. Phys. Lett.* **2014**, *104*, 013501.

[24] A. Kumar, T. M. Arruda, Y. Kim, I. N. Ivanov, S. Jesse, C. W. Bark, N. C. Bristowe, E. Artacho, P. B. Littlewood, C.-B. Eom, S. V. Kalinin, *ACS Nano* **2012**, *6*, 3841.

[25] F. Messerschmidt, M. Kubicek, J. L. M. Rupp, *Adv. Funct. Mater.* **2015**, *25*, 5117.